PERTANIKA 14(3), 359-371 (1991)

COMMUNICATION VII

A Subroutine Package for Solving Hydrodynamic Lubrication Problems

ABSTRAK

Kertas-kerja ini membentangkan satu perisian subrutin untuk menyelesaikan masalah pelincir hidrodinamik yang beroperasi dibawah saput sesuhu. Analisis dan algoritma pengiraan juga diterangkan. Kaedah unsur terhingga telah digunakan untuk menyelesaikan kedua-dua kes aliran lamina dan gelora. Satu contoh galas jara susuk tiga cuping digunakan untuk menunjukkan penggunaan perisian subrutin ini.

ABSTRACT

The paper presents a subroutine package that solves the problem of hydrodynamic lubrication operating under isothermal film. The underlying analysis and computational algorithm are described. The finite element method was used for solving the pressure equation for cases of both laminar and turbulent flow. A representative example of a three-lobe profile bore bearing is used to demonstrate the application of the subroutine package..

INTRODUCTION

The need to reduce machinery failure and maintenance costs while simultaneously increasing their power output and efficiency has led to numerous studies on ways of improving performance, reliability and life expectancy of critical machine elements. This has resulted in much development and advancement in design technology in the area of highly loaded rotating machinery particularly for elements such as bearings, cam followers and gear systems.

Advances in computer techniques in analysis have enabled the efficient numerical solution of lubrication problems. These include principally powerful numerical tools such as the finite difference method, the finite cell method and recently the finite element method. The most commonly used approach is the finite difference scheme. This method gives a point-wise approximation to the governing equations. The method, obtained by writing difference equations for an array of grid points, becomes more and more accurate as more points are considered. However, the finite difference scheme becomes inconvenient to use when irregular geometry or unusual boundary conditions are encountered. When complex geometrical configurations and abrupt changes in field properties are involved, the finite difference method becomes inherently difficult to apply because of the need to employ irregular meshes and special auxiliary conditions to implement the boundary conditions.

One of the newest and increasingly popular numerical techniques available today is the finite element method. This approach originated over twenty years ago in the aircraft industry as an effective means for analysing complex air frame structures (Zeinkewicz 1977). The method has been developed to include structural mechanics, metal forming, fluid mechanics and fluid film lubrication.

The use of the finite element technique for solving hydrodynamic lubrication problems was originally applied to field problems by Zeinkewicz and Cheng (1968). Booker and Huebner (1972) adopted the concept of a variational approach and a direct solution method for an infinitely long hydrodynamic bearing. Other researchers have expanded and developed the method. These include the works conducted by Gethin (1988) and more recently by Basri (1990) which are more user friendly.

This paper describes an analysis, the associated computational algorithm, and a resulting subroutine package developed to solve hydrodynamic lubrication problems.

Theoretical Basis

The Reynolds equation is fundamental to the analysis of hydrodynamic lubrication. By assuming that the bearing runs aligned and acounting isoviscous lubricant in the film, the turbulent Reynolds equation may be written (Ng and Pan 1975)

$$\frac{\partial}{\partial X}\left(\frac{h^3}{kx}\frac{\partial p}{\partial x}\right) + \frac{\partial}{\partial z}\left(\frac{h^3}{kz}\frac{\partial p}{\partial z}\right) = \mu U\frac{dh}{dx} \quad (1)$$

In equation (1), the quantities kx and kz are included to model non-laminar film and for moderate Reynolds number (< 5000) are given by Taylor (1923)

$$kx = \frac{1}{Gx} = 12.0 + 0.0039\,Re_T^{1.06} \quad (2)$$

$$kz = \frac{1}{Gz} = 12.0 + 0.0021\,Re_T^{1.06} \quad (3)$$

For turbulent flow the turbulent correction factors of Gz and Gx are included to give the volumetric flow terms as

$$Qx = \frac{Uh}{2} - \frac{h^3}{12\mu} Gx \frac{\partial p}{\partial x} \quad (4)$$

$$Qz = -\frac{h^3}{12\mu} Gz \frac{\partial p}{\partial x} \quad (5)$$

The Subroutine Package and Solution Procedures

The package consists of seven subroutines that compute the plain, cylindrical and multi-lode bearings, and a calling program. The programs are written in Fortran 90, are double precision, and self-contained. Parameters are passed between the calling program and subroutines through COMMON blocks.

The subroutines print the detailed solution at each time step, the intermediate results of iteration, and diagnostics in cases of failure. To facilitate plotting the results, the summary output is written in single precision into a separate file. These sets of source programs are about 4000 lines long.

The following set of boundary conditions was prescribed during the computational process:

(i) the condition that lubricant feed pressure is negligible in comparison with excursion in the film is reflected by the condition p(0, x) = 0. The position of the boundary where this condition holds is at the oil supply groove and it is also applicable at the downstream end of the pad which is also at a supply groove.

(ii) the pressure is ambient (i. e zero) along the bearing edge, then p(z, L/2) = 0

(iii) when appropriate and cavitation occurs, at the trailing edge the Swift-Steiber condition was applied i. e. at the cavitation boundary, zero gradient is satisfied by:

$$\frac{\partial p}{\partial z} = 0 \quad (6)$$

After the above boundary conditions were set up in the numerical model, the Reynolds or pressure equation was solved numerically. Each lobe of the bearing was divided into a finite number

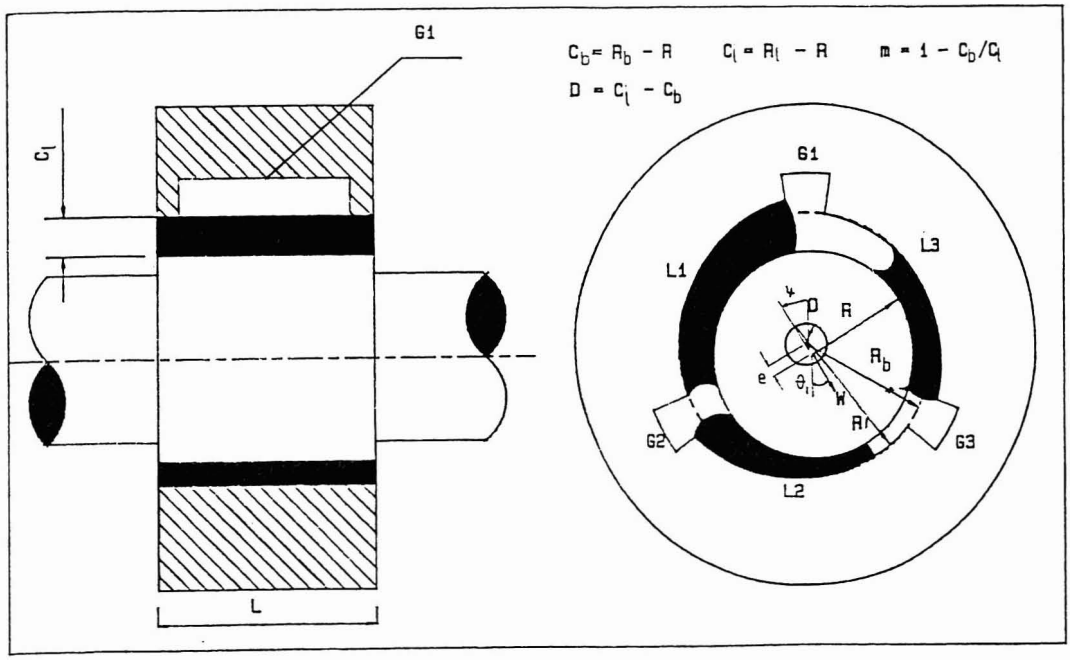

Fig.1: Bearing geometry and nomenclature for the numerical model

of eight noded isoparametric elements of the serendipity family as shown in *Figure 2* and throughout this study a mesh comprising 80 elements was used. Four elements were used in the half bearing length with twenty elements being employed in the direction of shaft rotation. The fine circumferential division was necessary to enable accurate calculation of the Swift-Steiber boundary condition.

The solutions for pressure distribution in the lubricant flow were obtained using an iterative scheme and the strategic steps in the solution procedure were the following:

(i) Define bearing geometry R, R_b, m, U, θ_t and θ and assume an initial bearing attitude angle φ.
(ii) Set-up initial pressure boundary conditions and the finite element mesh.
(iii) Calculate film thickness in each lobe of the bearing.
(iv) Solve the Reynolds or pressure equation.
(v) Continue the iteration for the pressure generation within the clearance gap of the bearing (i. e. steps iii and iv) until the agreement between two successive iterations at all points within the finite element mesh is better than 0.5%.
(vi) When step v has converged, by appropriate integration, the parameters which are of

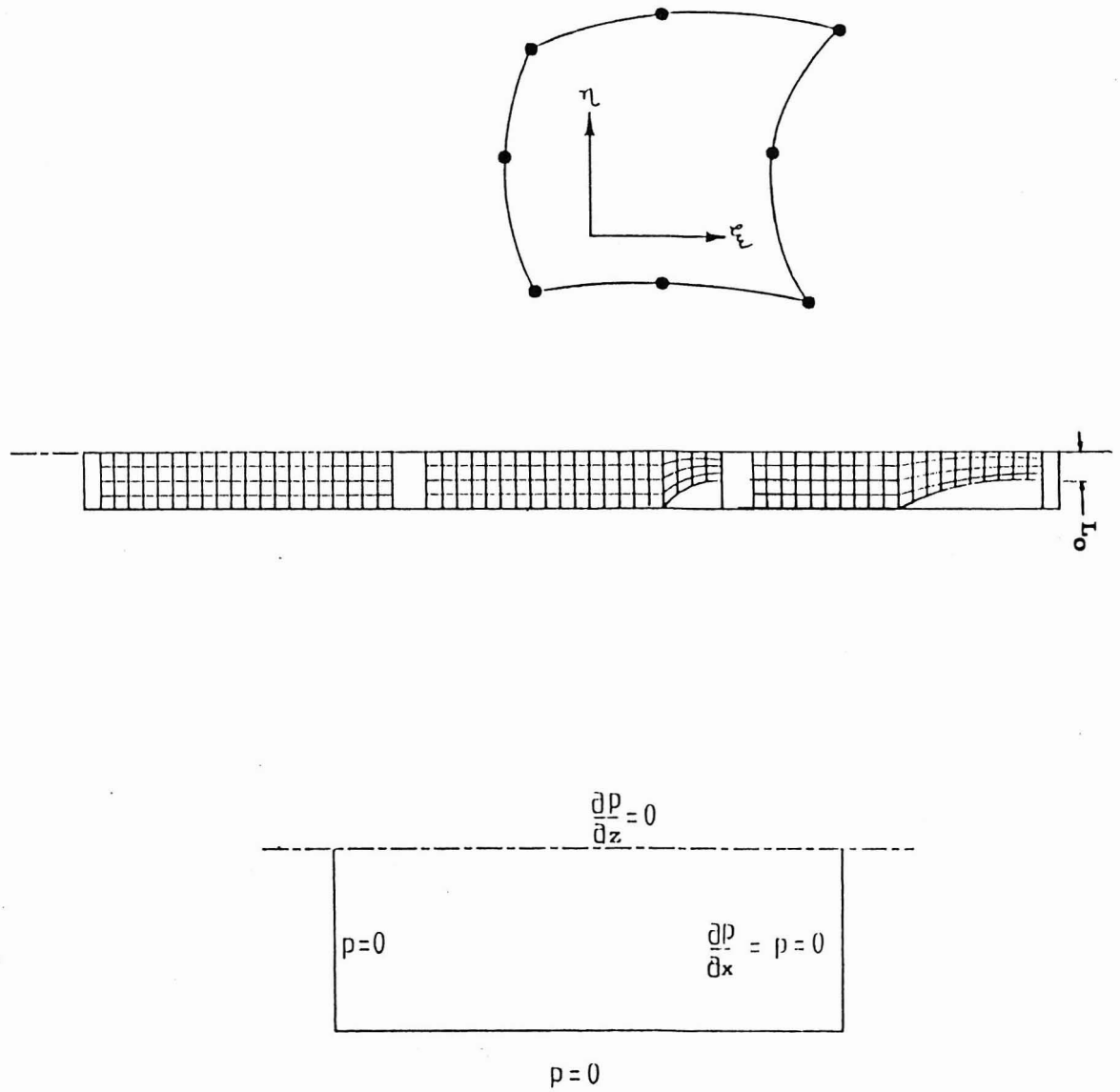

Fig.2: The finite element, mesh and associated boundary conditions

interest to the bearing designer (load carrying capacity, power loss and side leakage) are calculated by a simple summation over the bearing lobes.

The computer program developed for the turbulent calculation allows the assumption of either laminar, transition or turbulent flow within the gap depending on the magnitude of the local film Reynolds number. The change of flow type is carried out automatically in the course of the iteration process, whenever the local film Reynolds number value falls in the limit defined by the following bands (Frene and Constantinescu 1975)

$$Re_f < Rec1 \text{ and } Re_T = 0 \text{ (Laminar)} \quad (7)$$

$$Re_f \geq Rec2 \text{ and } Re_f = Re_T \text{ (Turbulent)} \quad (8)$$

and

$$Rec1 \leq Re_f \leq Rec2 \text{ and } Re_T = \frac{Re_f - Rec1}{Rec2 - Rec1} Re_f$$

(Transition) .....(9)

where

$$Rec1 = 41.2 \left(\frac{R}{C_b} \right)^{1/2} \quad (10)$$

while the establishment of fully turbulent flow the film Reynolds number is at twice Rec1, i. e.

$$Rec2 = 2\ Rec1 \quad (11)$$

TABLE 1
Global performance data

ϵ	S		ψ	
	1	2	1	2
0.100	1.234	1.234	60.09	60.24
0.310	0.353	0.355	61.00	61.20
0.429	0.181	0.182	59.46	60.02
0.702	0.085	0.086	55.23	55.70
0.806	0.054	0.055	51.68	51.92
0.882	0.034	0.036	47.19	47.19

$\overline{H}$		$\overline{Q}$	
1	2	1	2
1.424	1.432	0.134	0.135
1.478	1.479	0.147	0.147
1.574	1.577	0.165	0.168
1.794	1.796	0.189	0.191
2.016	2.208	0.207	0.209
2.290	2.293	0.232	0.231

1-data from Lund and Thomsen 1978 2-present data

Sample Computation and Discussion

From a design viewpoint, performance trends are essential to enable bearing selection for a particular engineering application. Therefore in this section, steady state design characteristics of a three-lobe profile bore bearing are presented.

Verification of the Numerical Models

Before proceeding with the parametric study, to confirm the basis of the mathematical model used in this paper, the computed global performance data for the basic bearing were compared with published data from Lund and Thomsen 1978 and Flack and Allaire 1982 and are presented in Table 1 and *Figure 3*.

It can be seen clearly that the baseline model developed (Table 1) shows complete agreement with published data which confirms its foundation with regards to this work.

Figure 3 illustrates a comparison of the computed dependence of eccentricity ratio on Sommerfeld number and is compared with published results by Flack and Allaire (1982) for various loading directions. Again, the graphical presentation shows the agreement of the present model with established work.

Parametric Study

A systematic series of calculations was completed for a range of present and loading vectors for symmetric and tilted configurations. The bearing had the following geometric details:

TABLE 2
Bearing geometries

$R = 37.41$ mm $R_b = 37.52$ mm

$C_b/R = 0.0003$

$\theta_g = 20°$

$\theta_t = O°$ and $40°$

Figures 4 and *5* show sets of dimensionless mid-plane pressure distribution in the symmetric and tilted three-lobe configuration for various loading vectors and for laminar turbulent calculations. Both figures show that for the loading direction of –60° and 60°, the predicted mid-plane pressure distribution is identical but indexed in a rotational sense. This is as expected and also confirms the basis of the numerical model. When turbulent flow is modelled, clearly the film pressures are higher and this is reflected in the

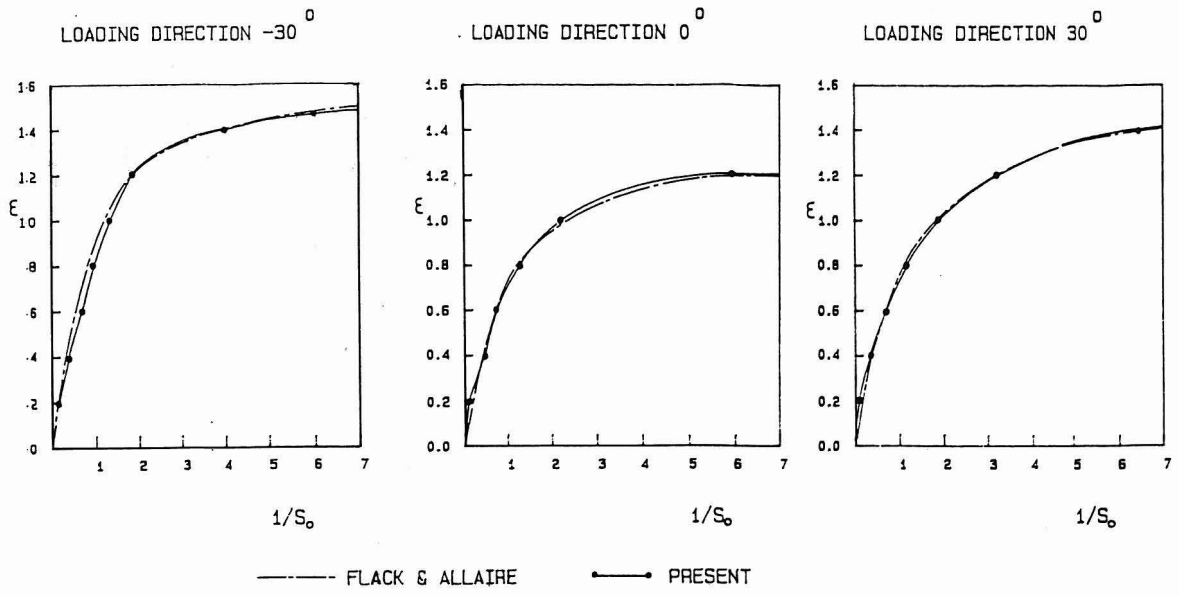

Fig. 3: Dependence of eccentricity ratio on Sommerfeld number for m=0.879 L/D=0.5 and C_b/R=0.0015: a comparison with published work

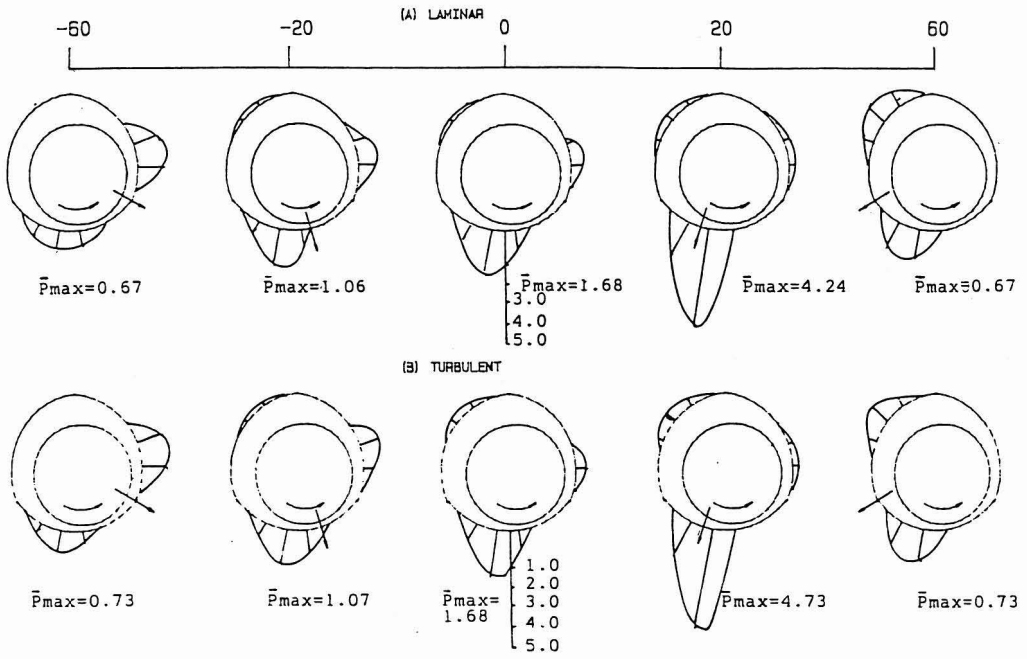

Fig. 4: Dimensionless film pressure distribution: N = 20000 rev/min; m = 0.8; symmetric bearing e/C_b = 0.8

global bearing behaviour as shown in *Figure 6*. For a loading directly on-pad ($\theta_1 = 0°$), the pressure is more significant in lobe 2 and almost negligible in lobes 1 and 3. For the symmetric bearing (*Figure 4*) it is apparent that the pressure is maximised when the loading vector is directed such that $\theta_1 = 20°$ clockwise, while for 40° tilted configuration (*Figure 5*) the pressure is maximised at a loading vector of

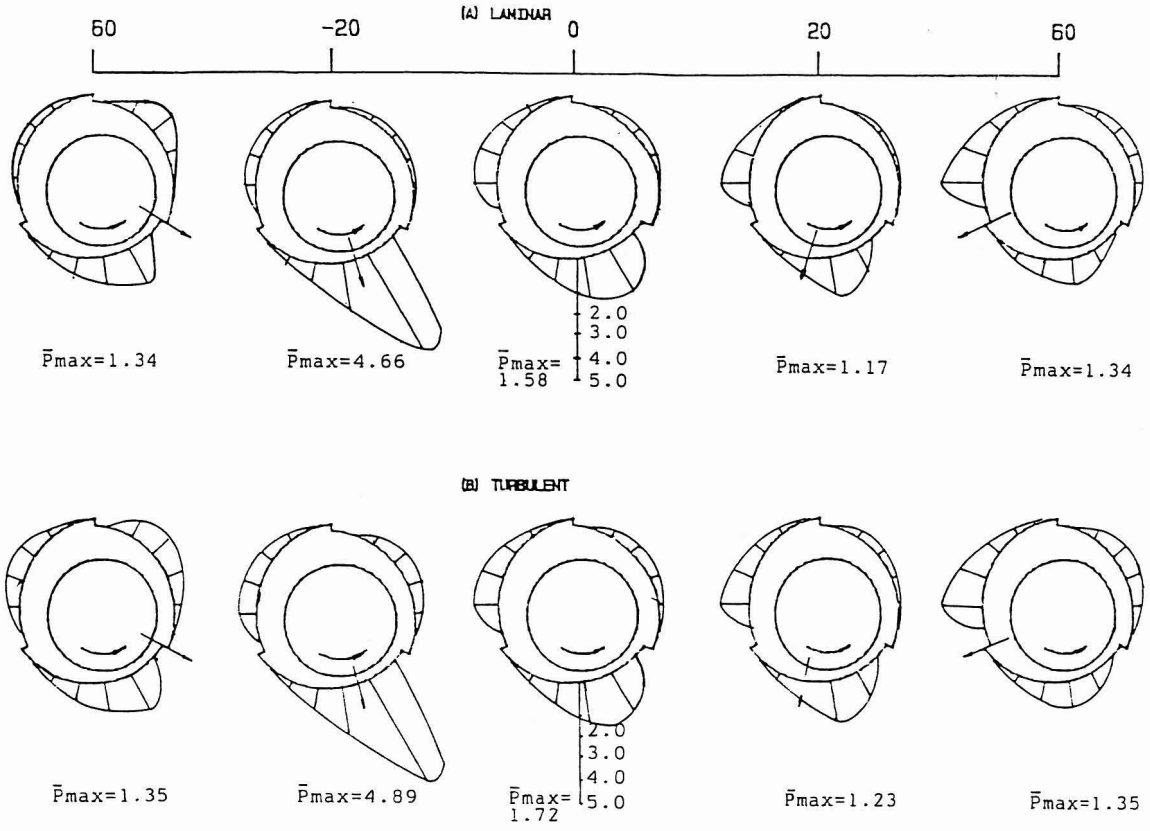

Fig. 5: Dimensionless film pressure distribution: N = 20000 rev/min; m = 0.8; tilted geometry $e/C_b = 0.8$

-20° counterclockwise. Under these conditions, the load carrying ability assumes its largest value. This occurs because the change in the film thickness in the loaded lobe is such that the Reynolds boundary condition is positioned at the downstream end of lobe 2. This condition is similar to that for the plain cylindrical bore geometry where the load-carrying ability is optimised when the loading vector is in the direction which is nearly orthogonal to the grooves. From the design viewpoint, this condition can be exploited to optimise the bearing performance on assembly by orienting the bearing appropriately.

Figure 6 illustrates the effects of including the turbulent flow correction factors in the pressure equation over a range of loading directions. It can be seen that the bearing global behaviour is identical in form to that for a laminar calculation but with enhanced load carrying capacity due to the increase in pressure generation. Power loss and leakage increased, the extent of which also depends on the nominal film Reynolds number. The shear stresses are higher when the flow is turbulent and this affects the higher power loss in the film under this flow condition. The flow is higher due to steeper pressure gradients generated at the edge of the film but, similar to the laminar flow condition, is independent of loading direction although the balance of flow from the different lobes changes with loading direction.

Figures 7(a) and *(b)* illustrate the load carrying ability for different tilt angles (θ_t) and presets (m) respectively for a range of loading directions. *Figure 7(a)* clearly shows a maximum value for a combination of tilt angle and loading direction and *Figure 7(b)* shows that for tilt angle θ_t of 40° presets affects load carrying ability but the maximum load carrying ability still occurs at the same loading direction. The position for maximum *(Figure 7(a))* lies where the loading direction is at –20° for tilt angle of 40°, 20° for symmetric bearing and 0° for tilt angle of 20°. *Figure 7(b)* illustrates the combination effect of preset (m) and loading direction for a fixed eccentricity ratio of 0.8 and tilt angle of 40°. A maximum is demonstrated for a loading direction of -20° and as with normal operation, load

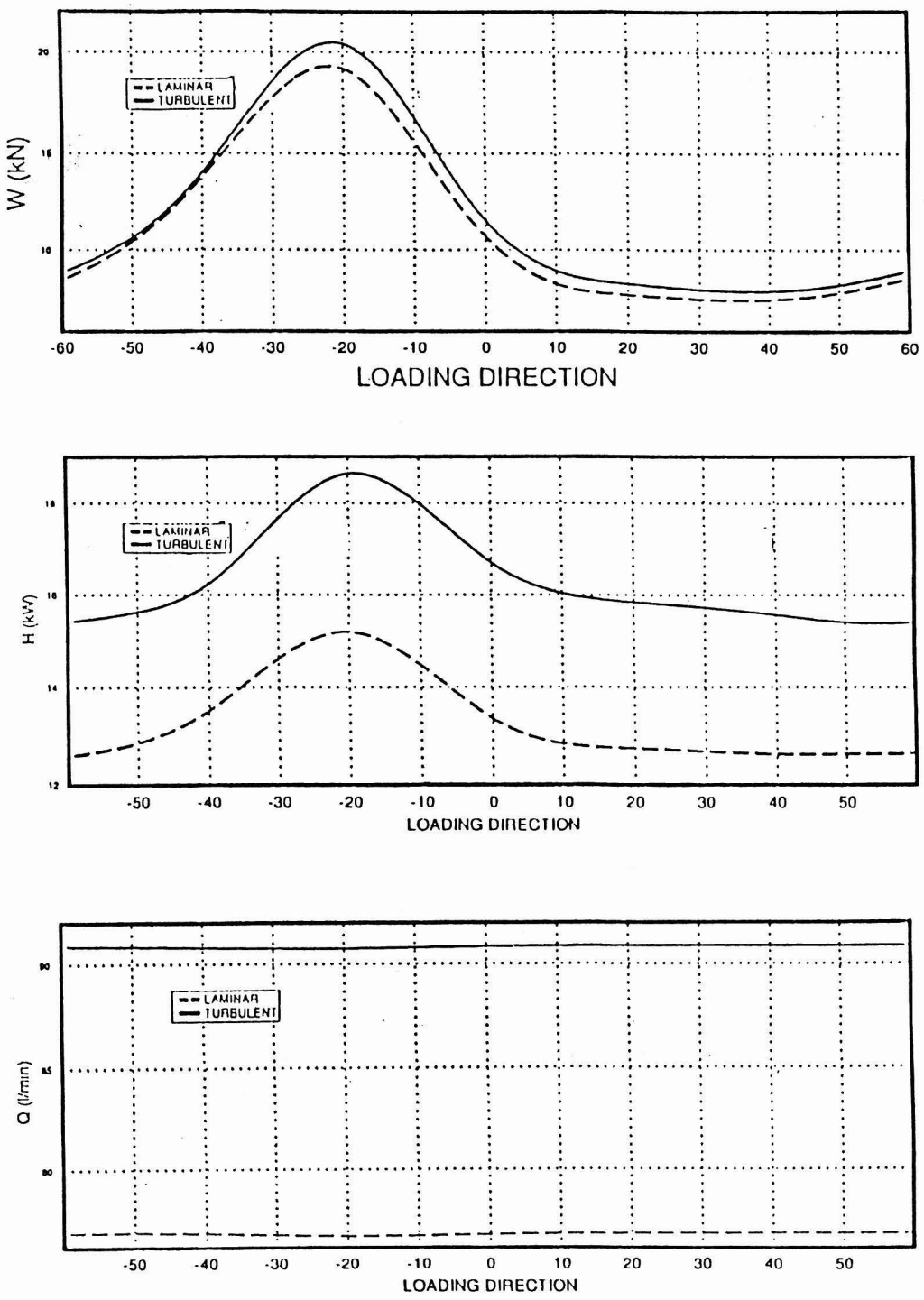

Fig. 6: Comparison between laminar and turbulent bearing behaviour at different loading direction: m = 0.85, N = 20000 rev/min; e/C_b = 0.8; re =393

carrying ability increases with increased preset. As explained previously, the maximum load occurs at this position due to thinner film in loaded lobe 2 and when Reynolds pressure boundary condition is positioned at the downstream end of this lobe, it consequently maximises the pressure generation.

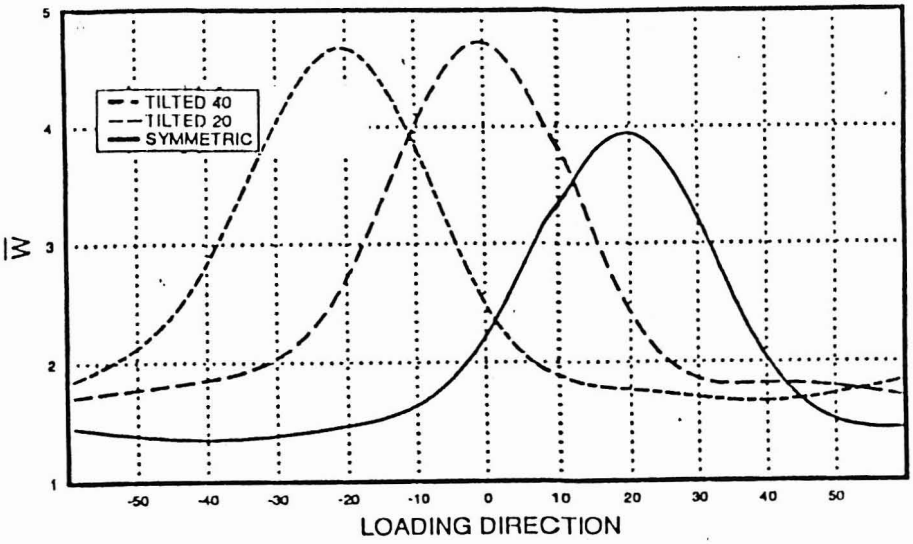

(A)

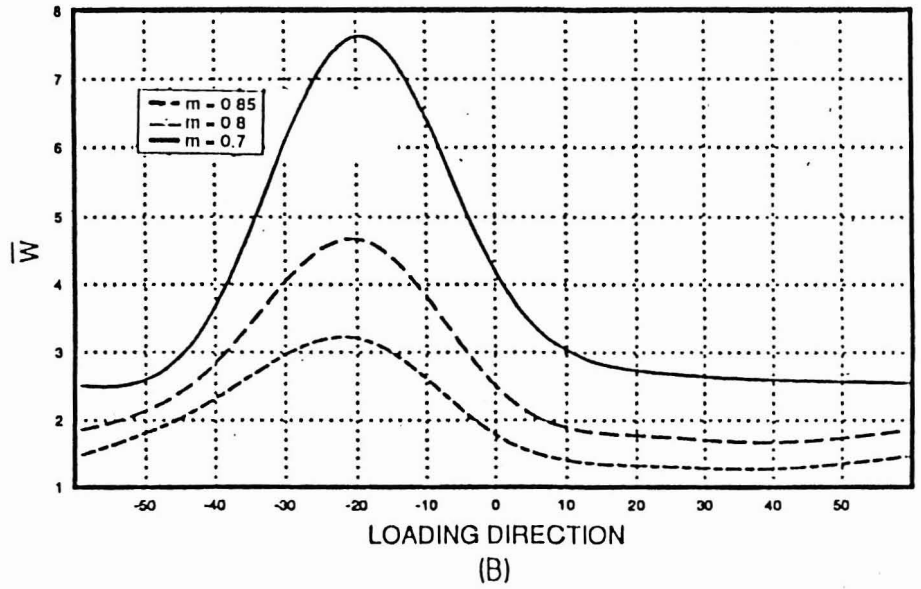

(B)

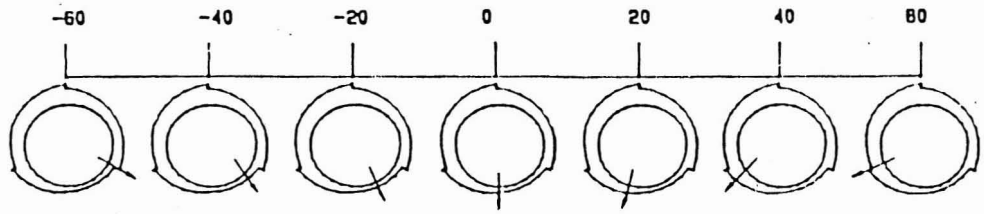

Fig. 7: Load carrying capacity at different loading direction: N = 20000 rev/min; e/C_b =0.8

Figure 8 shows the power loss in the bearing film. The losses in the bearing vary significantly with tilt angle and presets and are dependent on loading direction in a manner similar to the load carrying capacity. The condition of maximum loss occurs when loading vector is positioned at –20° for 40° tilt, 0° for 20° tilt and 20° for symmetric configuration . This occurs due to the high shear

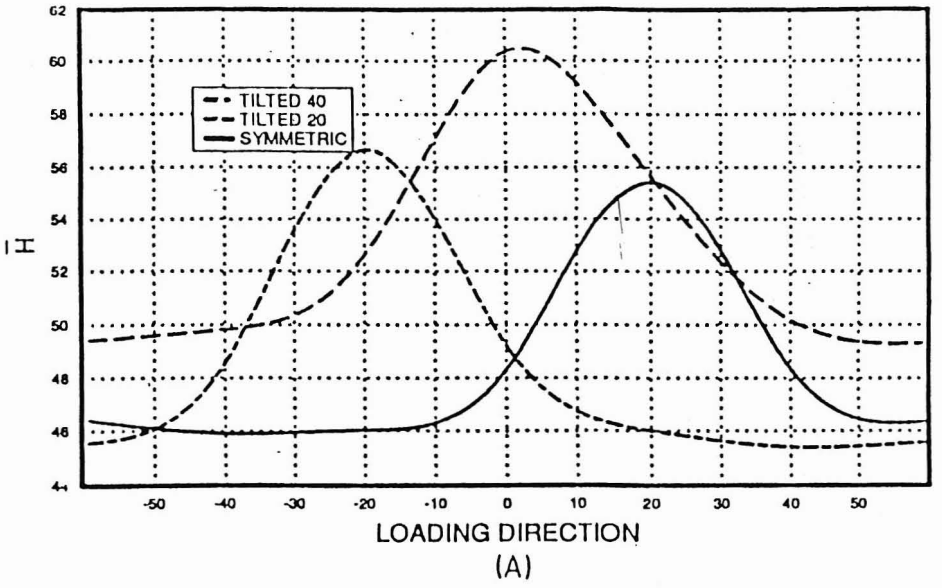

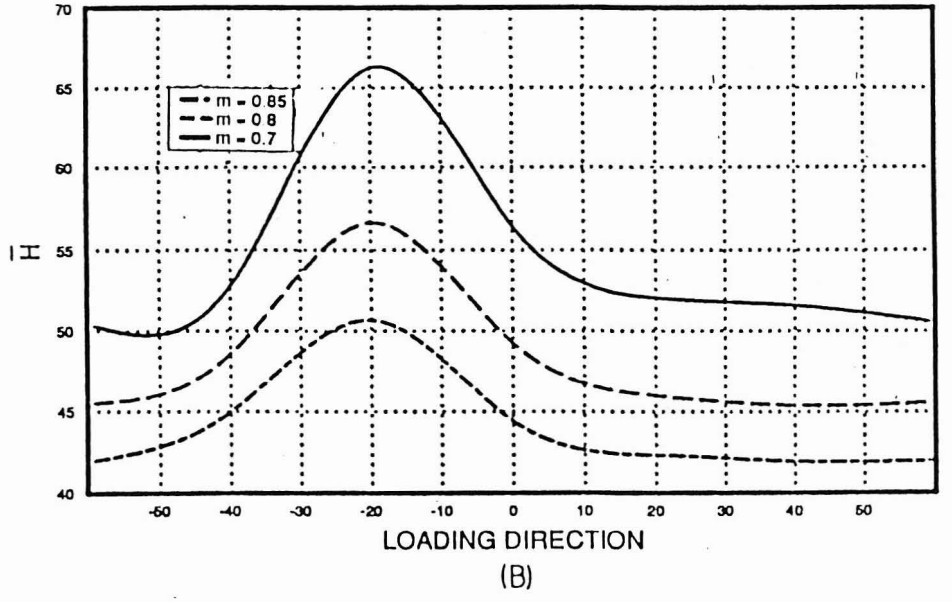

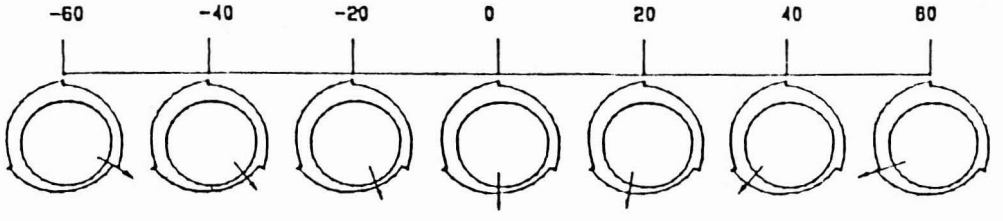

Fig. 8: Power loss at different loading direction: N = 20000 rev/min; e/C_b = 0.8

stress in lobe 2 which is fully wetted with a comparatively thin film is this region.

Dimensionless leakage is shown in *Figure 9* for a range of tilt angles *(9a)* and presets *(9b)*. The cumulative flow is independent of loading direction for the full range of tilt angles. However,

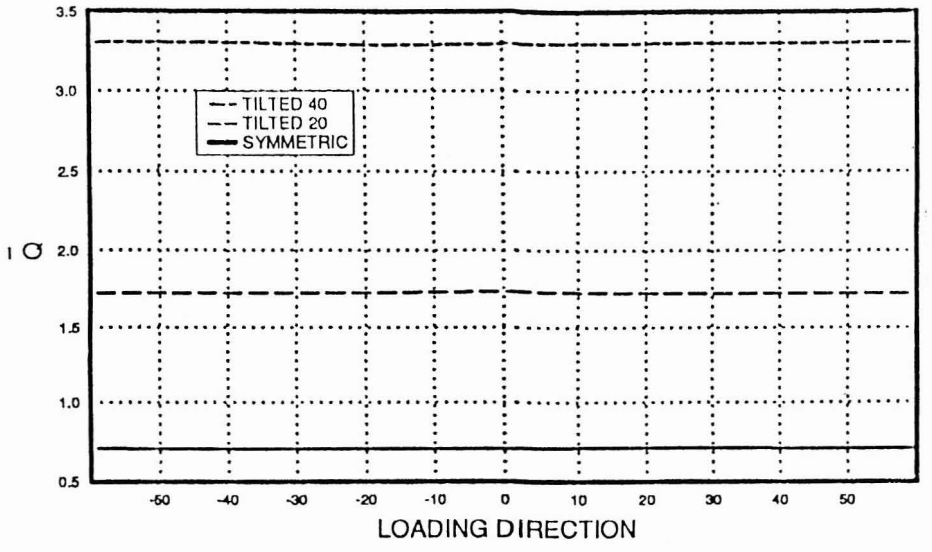

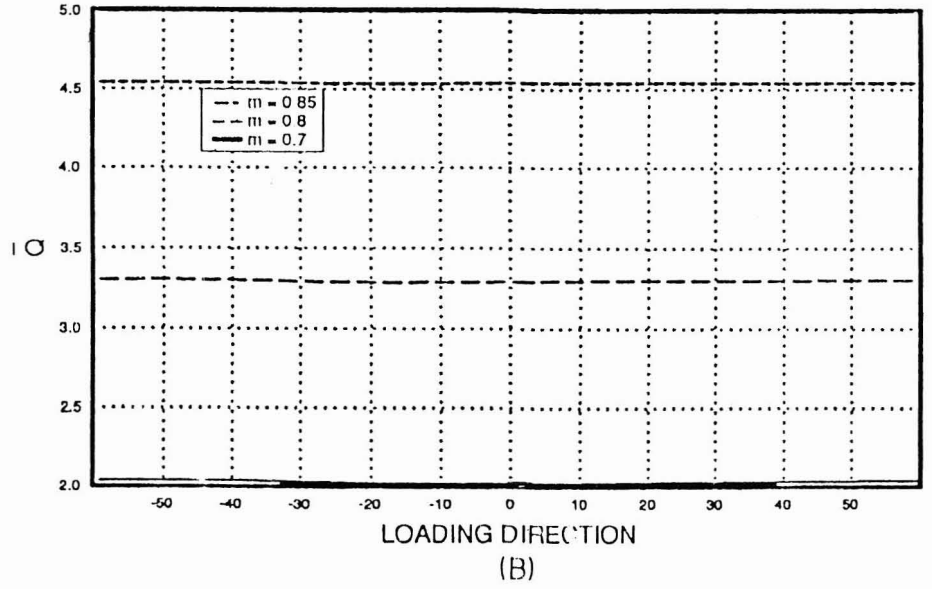

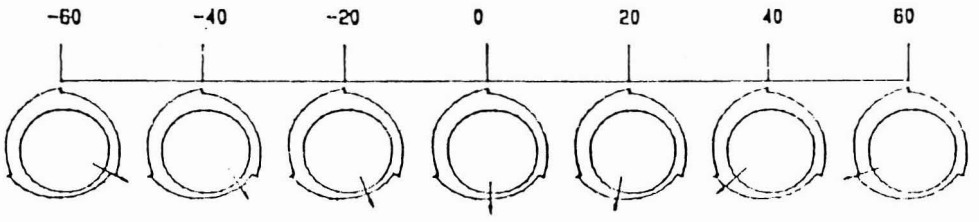

Fig. 9: Hydrodynamic leakage at different loading direction: N = 20000 rev/min; e/C_b = 0.8

the flow is increased when the tilt angle and preset are increased. This is due to the fact that when the preset is increased, the lobe radius (R_1) is also increased. For example, a bearing with an aspect ratio of 1.0, clearance ratio of 0.003, a shaft radius of 37.5 mm and preset of 0.8 will produce a lobe

radius equal to 38 mm; and a bearing with a preset of 0.7 will have a lobe radius of 37.78 mm. This shows that lobe clearance (C_1) is proportional to the bearing preset and therefore as the preset increases, the flow increases too. For this reason, the load-carrying capacity at high presets decreases, leading to improvement in heat removal characteristics.

To complete this set of data, *Figure 10* shows the change in attitude angles for laminar flow conditions and various loading directions. *Figure 10(a)* shows the bearing attitude angle for three types of profile configurations. For the tilted three-lobe bearing *(Figure 10(b))* the journal centre loci trends tend to shift towards positive attitude angle when position of loading is between –60° and –20°. However, between –20° to 10°, the attitude angle is negative. In view of rotordynamic bearing design, closeness between the line of centres and the load line reduces the susceptibility to film

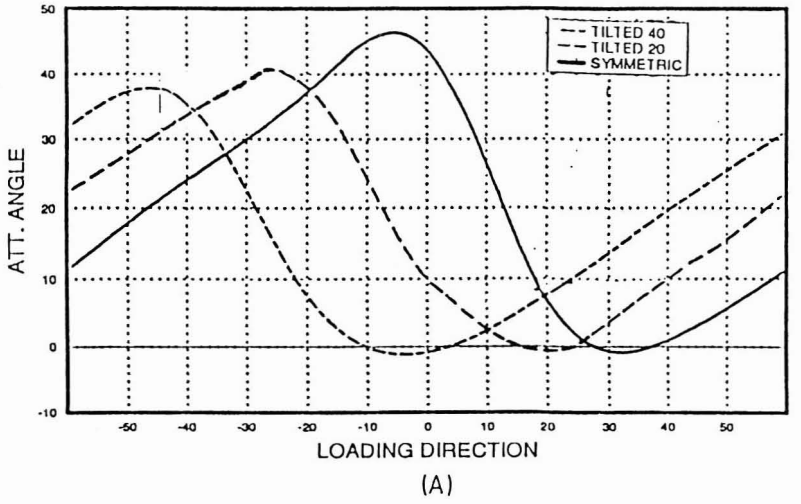

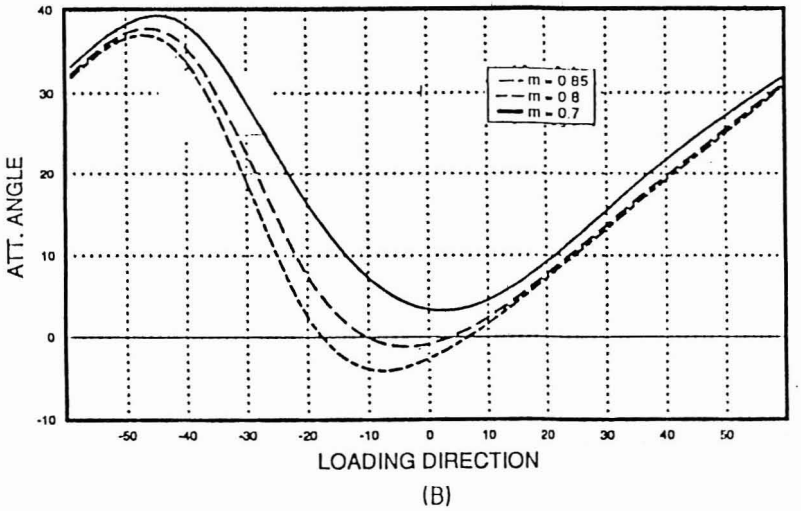

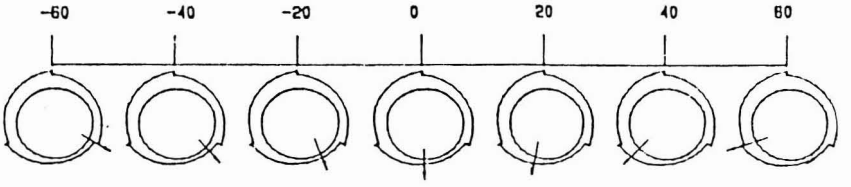

Fig. 10: Attitude angle at different loading direction: N = 20000 rev/min; e/C_b = 0.8

induced whirl.

To complete the set of data, Tables 3 to 5 present a small selection of dimensionless performance characteristics for tilted profile bore configuration so that precise values of the data are available for utilisation in computed-based design procedures similar to ESDU 84031and and ESDU 85028. It can be seen from the tables presented that even at moderate values of Reynolds numbers, turbulence can have a dramatic effect on the values of the global bearing performance compared with laminar operation particularly on the power loss.

TABLE 3
Dimensionless Load $\overline{W} = 1/S$

L/D=0.5			Re	
θ	0	500	1000	5000
–60	1.03	1.07	1.30	3.48
–40	1.60	1.64	1.93	4.74
–20	2.45	2.66	3.17	7.83
0	1.22	1.31	1.65	4.55
20	0.94	1.00	1.25	3.44
40	0.90	0.95	1.17	3.18
60	1.03	1.07	1.30	3.48
L/D=1.0				
–60	1.45	1.59	2.10	6.32
–40	2.27	2.37	2.95	8.35
–20	3.29	3.70	4.65	12.58
0	1.72	1.98	2.67	8.29
20	1.33	1.52	2.05	6.37
40	1.62	1.42	1.91	5.86
60	1.45	1.59	2.10	6.32

* computed at m = 0.85, ε = 0.80

CONCLUSION

A finite element model and a subroutine package have been developed and presented to predict the performance characteristics of hydrodynamic bearings. The numerical procedure is robust, easy to program and, since it uses fewer computations per iteration, is quite efficient. The underlying analysis is simplified by the assumption of constant density and viscosity lubricant. The algorithm the subroutine package has been successfully applied to a three-lobe profile bore bearing operating for various loading directions. Theoretical results are presented in nondimensional form and dimensional examples are given, including a comparison with published data. The agreement with published work is satisfactory.

SHAHNOR BASRI
Department of Mechanical and Systems Engineering

TABLE 4
Dimensionless power loss $\overline{H}$

L/D = 0.5		Re		
θ	0	500	1000	5000
–60	38.82	50.84	73.11	246.0
–40	40.80	52.44	74.46	246.4
–20	46.64	61.41	85.48	253.1
0	40.68	54.00	77.67	250.6
20	39.15	51.82	74.67	247.6
40	38.65	50.98	73.44	246.0
60	38.82	50.84	73.11	246.0
L/D = 1.0				
–60	42.01	56.44	82.84	284.9
–40	44.78	58.58	84.69	288.5
–20	51.03	68.05	97.32	311.6
0	44.18	60.68	87.76	291.1
20	42.45	58.02	84.37	288.1
40	41.96	56.45	83.03	285.2
60	41.01	56.44	82.84	284.9

*computed at m = 0.85, ε = 0.8

TABLE 5
Dimensionless Side Leakage $\overline{Q}$

L/D = 0.5		Re		
q	0	500	1000	5000
–60	8.190	9.134	9.345	9.869
–40	8.187	9.133	9.435	9.874
–20	8.167	9.121	9.399	9.854
0	8.176	9.120	9.414	9.852
20	8.180	9.125	9.426	9.857
40	8.184	9.129	9.433	9.862
60	8.190	9.134	9.436	9.869
L/D = 1.0				
–60	4.548	5.494	5.841	6.541
–40	4.545	5.487	5.832	6.450
–20	4.537	5.484	5.794	6.428
0	4.543	5.489	5.815	6.432
20	4.546	5.491	5.832	6.440
40	4.547	5.493	5.840	6.448
60	4.548	5.494	5.841	6.451

* computed at m = 0.85, ε = 0.8

Faculty of Engineering
Universiti Pertanian Malaysia,
43400 UPM, Serdang, Selangor Darul Ehsan,
Malaysia.

REFERENCES

BASRI, S.B. 1990. *Thermal Analysis of A Three-Lobe Profile Bore Bearing*, PhD Thesis, University of Wales, U.K.

BOOKER, J.F and K.H. HUEBNER. 1972. Application of Finite Elements to Lubrication: An Engineering

Approach. *Trans ASME (JOLT)* **24(4)**: 313-323.

FLACK, R. D. and P.E. ALLAIRE. 1982. An Experimental and Theoretical Examination of the Static Characteristics of Three Lobe Bearings. *Trans. ASLE* **25(1)**: 88-91.

FRENE, J. and V.N. CONSTANTINESCU. 1975. Operating Characteristics of Journal Bearings in Transition Regime. In *Proceedings of Leeds-Lyon Symposium on Tribology*, eds. Dowson, Godet and Taylor.

GETHIN, D.T. 1988. Finite Element Approach to Analysing Thermohydrodynamic Lubrication in Journal Bearings. *Tribology International* **21(2)**: 67-75.

LUND, J.W. and K.K. THOMSEN. 1978. *A Calculation Method and Data for Dynamic Coefficients of Oil-Lubricated Journal Bearings*, Special Publication of the American Society of Mechanical Engineers, No. 100118, New York.

NG, C.W. and C.H.T. PAN. 1975. A Linearized Turbulent Lubrication Theory *Trans. ASME Journal of Basic Engineering* **87**: 264-269.

TAYLOR, G.I. 1923. Stability of a Viscous Liquid Contained between Two Rotating Cylinders, *Phil. Trans. Roy. Soc. London*, **223(A)**: 289-343.

ZEINKEWICZ, O.C. 1977. *The Finite Element Method*, 3rd Edition, McGraw-Hill Publication.

ZEINKEWICZ, O.C. and Y.K. CHENG. 1968. Finite Elements in the Solution of Field Problems. *The Engineers* **24**: 507-510.

(Received 2 May, 1991)

NOTATION

C_b	Base clearance between the journal and bearing
C_l	Lobe clearance
D	Journal Diameter
D_b	Base Circle Diameter
G_x, G_z	Turbulent viscosity coefficient
H	Power loss
$\overline{H}$	Dimensionless power loss
L	Bearing length
N	Rotational Speed (rev/min)
P_f	Lubricant feed pressure
Q	Leakage
$\overline{Q}$	Dimensionless leakage
Q_{co}	Carried over lubricant
Q_f	Lubricant feed flow
Q_{in}	Lubricant at lobe inlet
Q_x	Flow per unit width in x-direction
Q_z	Flow per unit witdth in z-direction
R	Journal radius
R_b	Base Circle radius
R_l	Lobe radius
Re	Nominal Reynolds Number $(\frac{\rho UC}{\mu} b)$
Re_T	Turbulent Reynolds Number
Re_f	Local film Reynolds number
Re_{c1}	Reynolds number for onset of transition flow
Re_{c2}	Reynolds number for onset of turbulent flow
S_0	Sommerfeld number
TQ_B	Bush torque reaction
TQ_c	Bush torque reaction in the cavitated region
U	Sliding velocity
e	Eccentricity
h_l	Local film thickness in the bearing lobe
k	Turbulent correction factor
m	Preset
p	Film pressure
θ_1, θ_2, θ_3	Position of film commencement in each bearing lobe
θ_g	Groove angle
θ_l	Loading direction
θ_t	Tilt angle
ψ	Attitude angle
α	Angular position
ε	Eccentricity ratio $(=e/C_b)$
ε_1	Lobe eccentricity ratio $(=e_1/C_b)$
μ	Lubricant molecular viscosity
ν	Lubricant kinematic viscosity
ρ	Lubricant density
τ	Shear stress component
τ_c	Couette shear stress
ω	Rotational speed (rad/s)